Bioorganic Chemistry 91 (2019) 103158

Contents lists available at ScienceDirect

Bioorganic Chemistry

journal homepage: www.elsevier.com/locate/bioorg

Arylboronate prodrugs of doxorubicin as promising chemotherapy for pancreatic cancer

Charles Skarbek, Silvia Serra, Hichem Maslah, Estelle Rascol, Raphaël Labruère*

Institut de Chimie Moléculaire et des Matériaux d'Orsay (ICMMO), CNRS, Univ Paris Sud, Université Paris-Saclay, 15 rue Georges Clemenceau, 91405 Orsay Cedex, France

ARTICLE INFO

Keywords:
Prodrug
Doxorubicin
Reactive oxygen species
Anticancer chemotherapy

ABSTRACT

This study describes the synthesis of arylboronate-based ROS-responsive prodrugs of doxorubicin and their biological evaluation as anticancer agents. The determination of the most sensitive cancer type toward arylboronate prodrugs is crucial for further consideration of these molecules in clinical phase. To address this goal, an arylboronate-based profluorescent probe was used to compare the capacity of various cancer cell lines to efficiently convert the precursor into the free fluorophore. On the selected MiaPaCa-2 pancreatic cancer cells, a benzeneboronate prodrug exhibited 67% of the cytotoxicity obtained with the free doxorubicin. The prodrug was also able to induce tumor regression on MiaPaCa-2 pancreatic tumor model in ovo. Using this model, the amount of free doxorubicin liberated from this prodrug into the tumor was equivalent to the quantity measured after direct intratumoral injection of the same concentration of doxorubicin.

1. Introduction

Cancer caused more than 9 million deaths worldwide in 2018 and the number of new cases is constantly increasing [1]. Among different approaches, chemotherapy is largely used in medical oncology. Nonetheless, most of the currently employed chemotherapies against cancer are almost as toxic for the normal cells as for the tumor cells. Thus, there is an urgent need for the development of new and specific chemotherapies, capable of exploiting the differences between normal and tumor cells in order to increase the potency and therapeutic index by improving the balance between efficacy and toxicity [2]. During the last decades, the prodrug strategy has emerged, involving the development of activity-masked molecules designed for being rapidly activated through enzymatic or chemical reactions inside the tumors or within the tumor microenvironment. This approach ideally ensures a high selectivity against targets and low toxicity, since drugs are liberated specifically at the tumor area, generally by targeting the overexpression of enzymes or reactive oxygen species (ROS) surrounding the tumor, or the hypoxic environment of the tumor. Furthermore, the prodrug strategy remains faster than the development of novel therapeutic agents with appropriate drug-like characteristics [3].

Among various metabolic pathways, the activation of antitumor prodrugs by ROS seems particularly promising [4]. Biological study of tumors have revealed that cancer cells have a higher level of oxidative stress compared to healthy cells. This oxidative stress results in the overproduction of ROS including hydrogen peroxide (H_2O_2), hydroxyl radical ($HO^{\cdot}$) and superoxide anion ($O_2^{\cdot -}$). These ROS contribute significantly in different tumor progression processes such as cell proliferation and angiogenesis [5]. Neovascularization is a critical element of tumor metastasis since it allows access of certain cancer cells to the bloodstream leading to colonization of new organs [6]. In addition, H_2O_2 molecules produced in tumor cells will generate migration of these cells, which is also an important factor in the metastatic process [5].

Arylboronic acids and their corresponding esters have been widely used as temporary drug masking groups since activation is made possible by ROS (Scheme 1) [7,8]. These temporary moieties are triggered by H_2O_2, the most abundant and stable ROS produced by cancer cells, to further afford non-toxic boric acid [9]. Boronic acid groups were either directly linked to the drug or branched through a quinone methide-based self-immolative spacer. Oxidation of the carbon-boron bond will allow the formation of a hydroxy group. In the case of the self-immolative spacer, the latter electron donor function will cause electronic delocalization within the aromatic nucleus leading to the release of the drug [10]. Remarkably, arylboronic acid spacers are employed to link either alcohol or amine function-bearing drugs through ether, carbonate or carbamate bonds. The spacer is also commonly used to hinder the drug and allow a better masking of the

* Corresponding author.
E-mail address: raphael.labruere@u-psud.fr (R. Labruère).

https://doi.org/10.1016/j.bioorg.2019.103158
Received 11 June 2019; Accepted 24 July 2019
Available online 24 July 2019

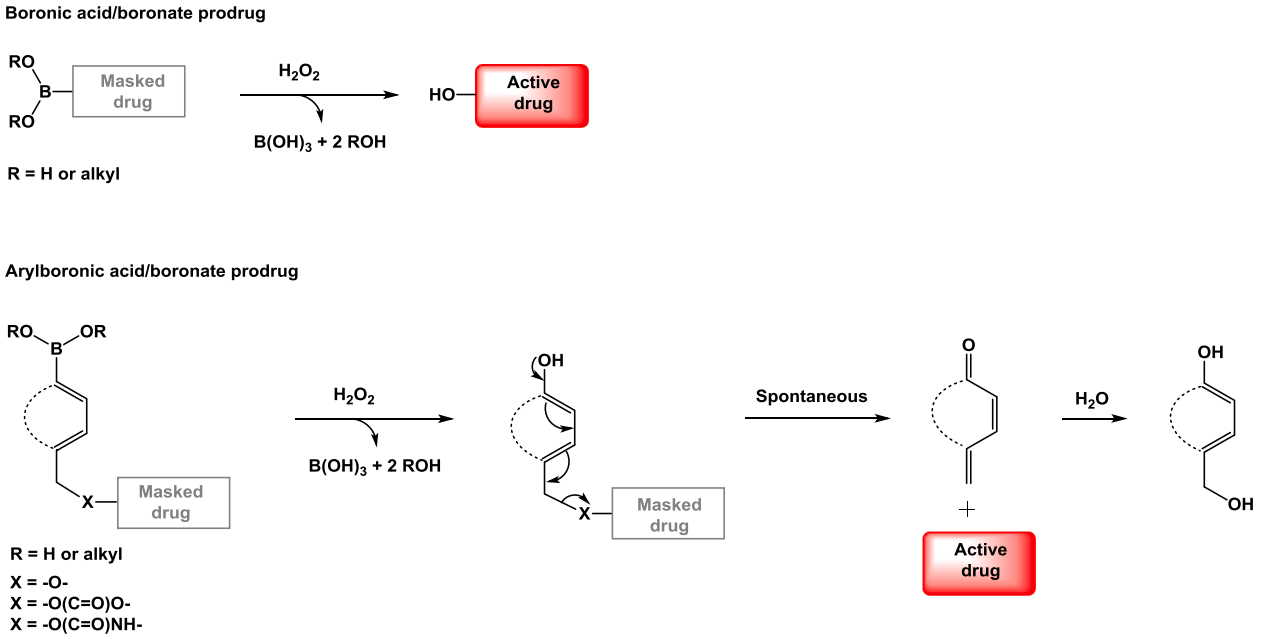

Scheme 1. Conversion of boron-containing prodrug into active drug.

biological activity.

This strategy has led to the development of probes for tumor imaging [11,12], ROS amplifiers [13–15] DNA cross-linking agents [16,17] and prodrugs of matrix metalloproteinase inhibitors [18], nitrogen mustards [19,20], camptothecin derivatives [21,22], endoxifen [23,24], methotrexate [25], cisplatin [26], HDAC inhibitors [27,28], 5-fluorouracil [29] and doxorubicin [30].

From this literature, we observed that the different arylboronic acid and ester precursors were evaluated on various cell lines with disparate cytotoxic results. The cancer cell line sensitivity to arylboronic prodrugs does not follow a clear trend from one study to another. In regards to a particular cell line, the structure of the arylboronic acid derivative has therefore a strong influence on the biological activity. The clear identification of the type of cancer sensitive to these boron-based prodrugs is central since none of these molecules has entered clinical trial so far. In this work, we decided to develop potent arylboronate-drug conjugates and further select the most receptive target among several cancer cell lines in order to identify the type of cancer that responds well towards these precursors. First, we selected doxorubicin (DOX), a good candidate for the design of prodrug. Indeed, DOX is a very effective antitumor drug with limited therapeutic efficacy due to stochastic repartition in the patient organs resulting in important cardiotoxicity [31]. Arylboronate-based self-immolative spacers were then used in order to branch the free amine function of DOX (Fig. 1). Several arylboronate moieties were used in order to study their influence on the kinetic of DOX release in presence of H_2O_2. Three different scaffolds were envisioned: (i) the unsubstituted benzeneboronate; (ii) a fluorinated benzene homolog since electron withdrawing atoms were shown to increase the kinetic of oxidation [32]; (iii) a furan ring, described as effective self-immolative spacer [33], to add a strong structural modification in comparison with the two aforementioned benzene moieties.

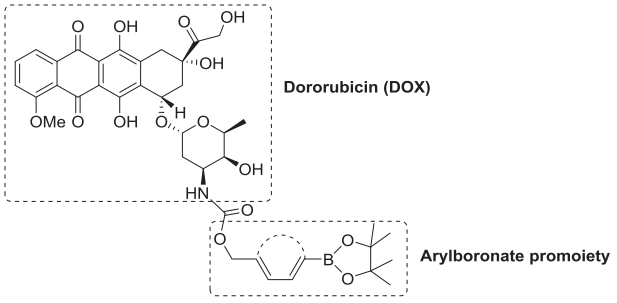

Fig. 1. General structure of the arylboronate prodrugs of doxorubicin.

Six cancer cell lines originating from different organs (breast cancer MCF-7 and the resistant counterpart MCF-7 MDR, hepatocellular carcinoma Hep G2, lung adenocarcinoma A549, glioblastoma U87, pancreatic cancer cell line MiaPaCa-2) were compared. An arylboronate profluorescent probe was used to determine the most effective cell line for the oxidation of the carbon-boron bond. Prodrugs of doxorubicin were then prepared and their cytotoxicity was assessed on the different cell lines. The most promising compound was further tested using in ovo tumor model via the HET-CAM (Hen's Egg Test-Chorioallantoïc Membrane) assay. This test has been widely used both for screening anticancer drugs [34–36] and for human tumor growth [37,38].

2. Results and discussion

2.1. Synthesis

The arylboronate profluorescent probe **3** was prepared in one step by reacting coumarin **2** with 4-bromomethylphenylboronic acid pinacol ester **1** in the presence of Cs_2CO_3 at room temperature for 4 h (Scheme 2).

Prodrugs **8a–c** were synthesized in two steps, starting from aryl alcohols **6a–c** (Scheme 3). Firstly, boronate **6b** was prepared through palladium catalyzed bromine-boron exchange starting from compound **4** [39]. Ester **6c** was obtained in 79% yield by reacting commercially available boronic acid **5** with pinacol in THF. Alcohol activation of **6a–c** was carried out in presence of 4-nitrophenyl chloroformate to provide activated compounds **7a–c**. DOX was then linked to the arylboronate promoiety through its amine group using an addition-elimination reaction to afford prodrug **8a–c**. A similar reaction was used to prepare the control molecule **9**, a benzeneboronate precursor of non-toxic phenylalanine. Another control molecule, the carboxylic acid **12** which is a bioisostere derivative of **8a**, unable to liberate DOX was prepared: (i) activated carbonate **11** was obtained from commercially available 4-(hydroxymethyl)benzoic acid **10** in 74% yield; (ii) DOX was then branched according to an addition-elimination reaction (Scheme 3).

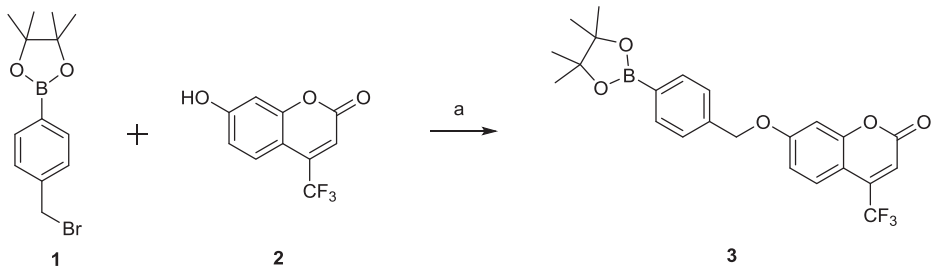

Scheme 2. Synthesis of the arylboronate profluorescent probe **3**. Reagents and conditions: (a) Cs_2CO_3, DMF, r.t., 4 h.

2.2. H_2O_2 activation of the profluorescent probe

The in vitro activation of arylboronate profluorescent probe **3** was carried out using increasing equivalent of H_2O_2 (1, 5, 10 and 50 equivalents). We recorded the temporal evolution of the free coumarin **2** fluorescence after oxidation and further self-immolation from

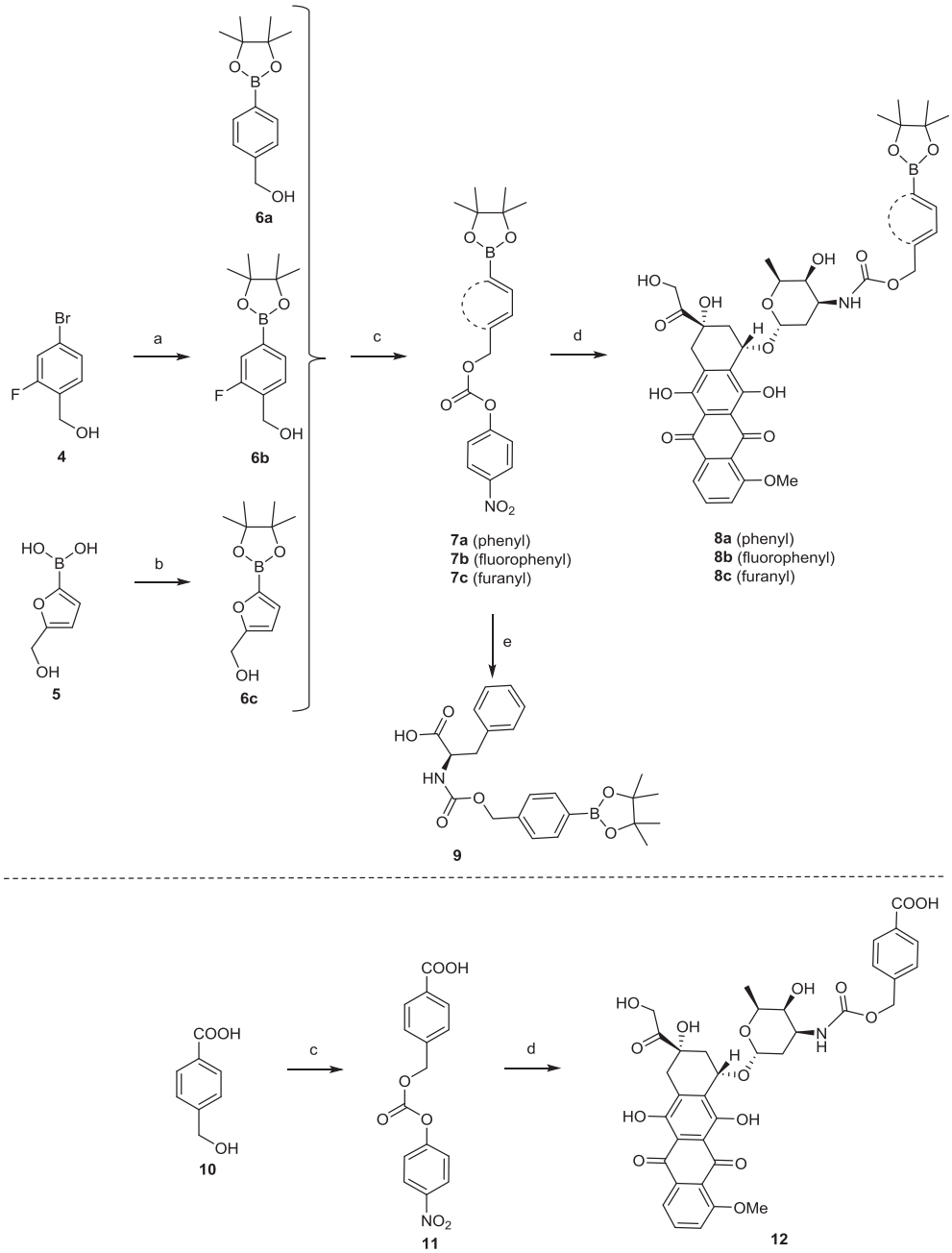

Scheme 3. Synthesis of boronate prodrugs and controls. Reagents and conditions: (a) AcOK, $Pd(dppf)Cl_2{\cdot}CH_2Cl_2$, $B_2(Pin)_2$, DMF, 80 °C; (b) pinacol, THF, 40 °C; (c) 4-nitrophenyl chloroformate, base, DCM, 0 °C to r.t.; (d) DOX·HCl, HOBt, Et_3N, DMF, r.t.; (e) phenylalanine, HOBt, Et_3N, DMF, r.t.

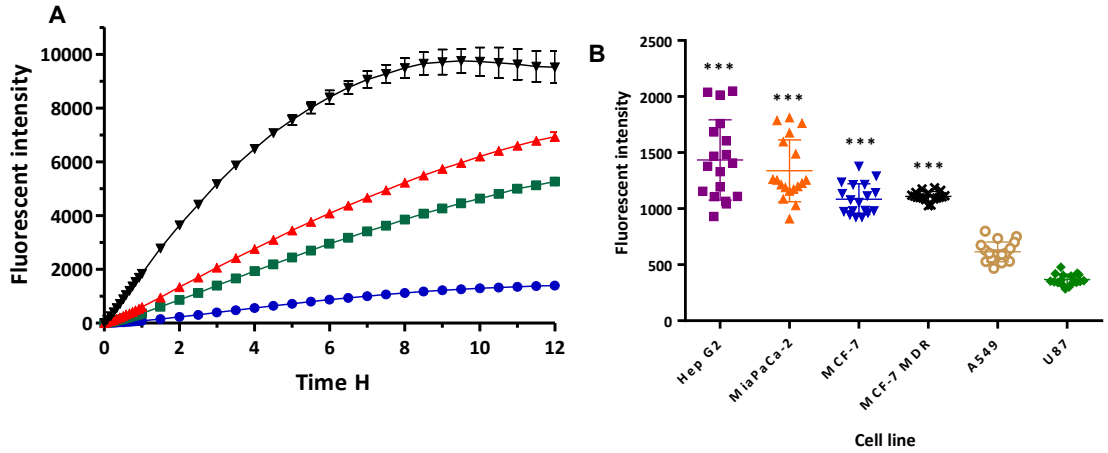

Fig. 2. (A) Coumarin release from the arylboronate profluorescent probe **3** in presence of H_2O_2 (▼ 50 eq., ▲ 10 eq., ■ 5 eq. and ● 1 eq.). (B) Investigation of the capacity of ROS production by cell lines (*statistically significant difference compared to U87 cell line with $p < 0.0001$).

precursor **3** (Fig. 2A). We observed that high concentrations of H_2O_2 led to the fastest kinetic of coumarin release. The use of 5, 10 and 50 equivalents led to the highest fluorescence release with half time values of 5.5, 5 and 2.5 h, respectively. As expected, these results showed a bimolecular kinetic of oxidation for our benzeneboronate profluorescent probe **3**. The use of equimolar quantity of H_2O_2 leads to slow release of coumarin in line with the known sluggish kinetic of reaction between benzeneboronate and H_2O_2 [40]. Moreover, the release is slowed down since the coumarin is linked to the self-immolative spacer via an ether link [41].

2.3. Cell line screening

The capacity of each tested cell line to produce ROS was measured using the benzeneboronate profluorescent probe **3**. The slow kinetic profile of disassembly is essential to generate enough contrast between the different cell lines toward their ability to produce different level of ROS. After six hours of incubation with each cell line, the release of coumarin from **3** was quantified by spectrofluorimetry (Fig. 2B).

This intensity relates the ability of each tested cell line to produce the ROS responsible for the oxidation of the boron-carbon bond leading to the release of coumarin. Since oxidation and subsequent self-immolation of precursor **3** is rather slow and dependent of the ROS concentration, we chose to: (i) incubate **3** in the presence of a large number of cells in order to produce as much ROS as possible using six-well plates; and (ii) maintain contact for 6 h to obtain a significant amount of liberated coumarin. The A549 and U87 cell lines demonstrated a low production of ROS as only a weak fluorescence intensity was observed. On the other hand, Hep G2, MiaPaCa-2, MCF-7 and MCF-7 MDR revealed a higher production of ROS as the fluorescence intensity was much higher compared to the other tested cell lines. Further, Hep G2 and MiaPaCa-2 were the most active cell lines for conversion of precursor **3** into coumarin **2** and these two cell lines seem to be the most suitable for further investigation of ROS-activatable prodrugs. The comparison of the ROS production by these cancer cells versus the cell line producing the least ROS (U87) was unequivocal and confirmed using a Kruskall-Wallis test with $p < 0.0001$.

2.4. In vitro cytotoxicity

As opposed to the probe **3**, the prodrugs are built of an aryl self-immolative spacer bonded to DOX through a carbamate linker to enhance the kinetic of disassembly [41] as it is beneficial for the biological activity to release high level of drug rapidly (data not shown). The IC_{50} of all the designed prodrugs (**8a–c**) and controls (**9** and **12**) were evaluated on the panel of cell line and the results are depicted in Table 1. No activity was observed on the multidrug resistant cell line MCF-7 MDR. DOX showed an important cytotoxic activity on all the other tested cell lines with nanomolar IC_{50} ranging from 10 to 600 nM. The cell lines U87, MCF-7, Hep G2 and MiaPaCa-2 were sensitive to DOX with IC_{50} around 100 nM. A549 cell line on the other hand demonstrated a lower activity with an IC_{50} of 600 nM. The control compounds **9** and **12** had no activity on the studied cell lines even at our highest tested concentration of 50 μM. These results are coherent as these control molecules have no trigger unit (**12**) or deliver a non-toxic motif (**9**).

All the ROS-activatable doxorubicin prodrugs (**8a–c**) demonstrated activities on the DOX-sensitive cell line and variable micromolar activities were obtained ranging from 0.1 to 10 μM underlining moderate activities of the tested prodrugs. The activity of the different prodrugs on a particular cell line was comparable except in the case of MiaPaca-2 where **8a** was more cytotoxic than **8b** and **8c**. Interestingly, **8a** showed activity on the MiPaCa-2 cell line with an IC_{50} close to the one obtained with the free DOX, 0.3 μM for **8a** versus 0.2 μM for DOX. Although the conversion of **8a** is not complete: ~67%, as deducted from the activity obtained with the same concentration of free doxorubicin, we observe a greater conversion than those obtained for related structures (~40%) [22]. **8a** was however not as active against the Hep G2 cells (IC_{50} = 4 μM, ~4% estimated conversion), a cell line able to produce similar level of ROS as the MiPaCa-2 cell line. As described by Doskey et al. [42], the H_2O_2 removal rate constants differ greatly between cell lines. In exponential growth phase, Hep G2 cells were shown to remove H_2O_2 four times faster than the MiaPaCa-2 cells. In our study, the cytotoxic activities were determined after 72 h of incubation when cells have reached their exponential growth phase and this can therefore rationalize the strongest activity of **8a** against MiaPaCa-2 in comparison with Hep G2 cell lines.

2.5. Chick chorioallantoic membrane (CAM) assay and HPLC detection of DOX

The HET-CAM assay was developed to investigate the efficacy of our most active arylboronate doxorubicin prodrug **8a** using the MiaPaCa-2 pancreatic cancer cell line for tumor production on the CAM as it showed the most promising cytotoxicity and an elevated release of ROS. Different protocol of intratumoral injection of **8a** or DOX were performed. In our case and according to the literature, we first determined the highest dose of DOX that was not lethal for the embryo [36]. Our maximum dose of 184 nmol (100 μg) of DOX in a single injection was well tolerated in a statistically significant sample size of chick embryos. For the evaluation of the tumor regression, we chose to enhance the number of injections rather than testing a high concentration as a single

Table 1
In vitro cytotoxicity of **8a–c**, **9** and **12** on the different cell lines. Percentage of restored activity is displayed in bracket. Nd: Not determined.

Cell line	IC_{50} (μM) ± SD				
	DOX	**8a**	**8b**	**8c**	**9/12**
U-87	0.10 ± 0.02	4.50 ± 0.40 (2%)	Nd	3.50 ± 0.20 (3%)	> 50
A-549	0.60 ± 0.10	11.10 ± 0.80 (5%)	8.40 ± 0.90 (7%)	4.30 ± 0.35 (14%)	> 50
MCF-7	0.09 ± 0.01	3.00 ± 0.20 (3%)	7.80 ± 0.50 (1%)	4.90 ± 0.60 (2%)	> 50
MCF-7 MDR	> 50	> 50	> 50	> 50	> 50
MiaPaca-2	**0.20 ± 0.00**	**0.30 ± 0.01 (67%)**	8.30 ± 0.70 (2%)	1.20 ± 0.20 (17%)	> 50
Hep G2	0.15 ± 0.02	4.00 ± 0.40 (4%)	7.70 ± 0.40 (2%)	3.40 ± 0.20 (4%)	> 50

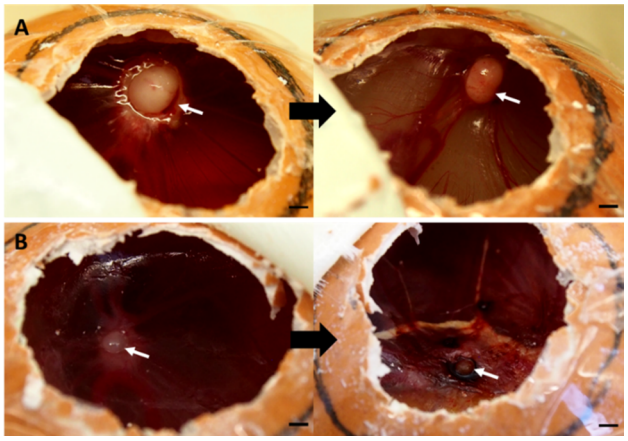

Fig. 3. In ovo efficacy of **8a** compared to DOX after two intratumoral injections of each drug (20 nmol) twice a day for two consecutive days, white arrows indicate the tumors, scale bar: 0.5 cm. (A) left: tumor before injection of DOX; right: tumor three days post injection of DOX (50% tumor regression). (B) left: tumor before injection of **8a**; right: tumor three days post injection of **8a** (tumor necrosis and 50% regression). Image treatment and tumor measurements were fulfilled using FIJI software [43].

dose taking into account the poor solubility of **8a**. Optimized protocol was found with the administration of DOX or **8a** (20 nmol) intratumorally twice a day and two days in a row followed by an observation of the tumor size after three days. This protocol led us to observe a significant decrease of the tumor in DOX group (~50% regression) and a comparable result was obtained for **8a** (~50% regression) (Fig. 3). Statistically relevant images of MiaPaCa-2 tumor implanted on the CAM are shown in Fig. 3. Necrosis seen in Fig. 3**B** was noticed in several experiments as the result of DOX/**8a** action. In this vascularized tumor model, the tested drug has also some antivascular effect often leading to partial necrosis of the tumor.

In order to confirm that the prodrug activity was due to its conversion into free DOX, a HPLC method for the measurement of DOX concentration in the tumors was elaborated. Tumors were extracted from the chorioallantoic membrane and sonicated to recover the free DOX. The same amount of DOX was found in both groups (30% of the initial dose) which is coherent with the tumor regression observed in ovo whereas prodrug **8a** was not detected. These results show that, in presence of a well-developed tumor, the prodrug **8a** is converted into DOX.

In this study, no strong tumor regression or total resection was observed. Indeed, in the HET-CAM assay, the dose escalation is difficult to study as it can lead to the death of the embryo resulting in a false positive result. Taking into account the ethical regulation and the small window between the drug injection and the end point before the embryo's birth, observation of tumor evolution over a long period is not possible. Therefore, we were able to only monitor partial regression of the tested tumors.

3. Conclusion

A profluorescent probe was used to select a cancer cell line strongly producing ROS. Among the six cell lines tested, Hep G2 and MiaPaCa-2 were the most effective at oxidizing the benzeneboronate probe. Prodrugs of doxorubicin and controls were then synthesized and their cytotoxic activity was determined in vitro on our panel of cell lines. Prodrug **8a** was selectively active on pancreatic cancer cells MiaPaca-2 with a recovery of 67% of the activity of the free doxorubicin. Further testing in ovo allowed us to observe the behavior of this prodrug on a MiaPaCa-2 tumor model. Similar tumor regression was observed using the same dose of both the prodrug **8a** and the free drug counterpart on the available timescale of reading. Quantification of the doxorubicin released from **8a** by oxidation in pancreatic tumor in ovo confirmed the latter result. The development of benzeneboronate-containing prodrugs must be pursued for the treatment of certain cancer types and we herein highlighted the promising potential of such prodrug in the treatment of pancreatic adenocarcinoma.

4. Experimental section

4.1. Synthesis

All chemical reagents were of analytical grade, obtained from Acros, Alfa Aesar, or Aldrich, and used without further purification. Solvents were obtained from SDS or VWR-Prolabo. Dichloromethane (DCM) was dried on molecular sieves and used immediately. Chromatography was performed using silica gel (35–70 μm, Merck). Concentration of solutions was performed under reduced pressure at temperature below 40 °C using rotary evaporator. Analytical TLC was performed using Silica Gel 60 F_{254} pre-coated aluminum plates (Merck). Spots were visualized by treatment with ninhydrine revelator followed by heating and/or by absorbance of UV light at 254 nm or fluorescent light at 360 nm. NMR spectra were collected on Bruker DPX 250 (^{1}H at 250 MHz and ^{13}C at 62.5 MHz), AV 300 (^{1}H at 300 MHz and ^{13}C at 75 MHz) or AV 360 (^{1}H at 360 MHz and ^{13}C at 90 MHz) spectrometers and analyzed using MestReNova software. Chemical shifts are reported in ppm (δ) and coupling constants in Hz (J). NMR spectra were performed in $CDCl_3$ or $(CD_3)_2SO$. High-resolution mass spectrometry (HRMS) analyses were performed by electrospray with positive or negative (ESI^+ or ESI^-). The purity of all compounds used for biological activity test was checked by reverse phase analytical HPLC and confirmed to be ≥95%.

4.2. Compound 3

To a solution of bromo derivative **1** (41 mg, 0.13 mmol), coumarin **2** (30 mg, 0.13 mmol) in 5 mL of DMF was added Cs_2CO_3 (46 mg, 0.14 mmol). The reaction was kept under agitation at r.t. for 4 h before being quenched with a saturated solution of $NaHCO_3$. The suspension was extracted with EtOAc (3 × 20 mL), the organic layers were combined, washed with brine, dried with $MgSO_4$, and concentrated under reduced pressure to give a crude product. The crude product was purified by column chromatography over silica gel with Cyclohexane-EtOAc: 100-0 to 60-40 to give the expected product as a white solid (35 mg, yield: 60%).

^{1}H NMR (300 MHz, $CDCl_3$) δ 7.85 (d, J = 8.0 Hz, 2H), 7.63 (dd, J = 9.0, 1.8 Hz, 1H), 7.43 (d, J = 8.0 Hz, 2H), 6.99 (dd, J = 9.0, 2.6 Hz, 1H), 6.93 (d, J = 2.5 Hz, 1H), 6.62 (s, 1H), 5.19 (s, 2H), 1.35 (s, 12H). ^{13}C NMR (75 MHz, $CDCl_3$) δ 162.45, 161.23, 159.37, 156.20, 138.35, 135.23, 126.54, 126.38, 123.43, 119.77, 113.99, 112.38, 107.23, 102.49, 83.92, 70.51, 24.84. HRMS (ESI): *m/z* Calcd for $C_{23}H_{22}BF_3O_5Na$, $[M+Na]^+$: 469.1410, found: 469.1409.

4.3. Compound 7a

To a solution of 4-nitrophenyl chloroformate (264 mg, 1.26 mmol) in 3 mL of DCM at 0 °C was added dropwise Et_3N (177 µL, 1.26 mmol). The mixture was stirred during 20 min under argon then a solution of **6a** (100 mg, 0.42 mmol) in 4 mL of DCM was added dropwise to the first solution and the mixture was stirred during 3 h at r.t. The reaction was quenched with brine, extracted with DCM (3 × 20 mL), the organic layers were combined, dried with $MgSO_4$ and concentrated under reduced pressure to give a crude product. The crude product was purified by column chromatography over silica gel with cyclohexane-EtOAc: 90-10 to 60-40 to give the expected product (135 mg, yield: 80%).

^{1}H NMR (300 MHz, $CDCl_3$) δ 7.88–7.82 (m, 2H), 7.46–7.41 (m, 2H), 7.40–7.35 (m, 2H), 5.31 (m, 2H), 1.35 (s, 12H). ^{13}C NMR (75 MHz, $CDCl_3$) δ 155.47, 152.38, 145.36, 137.02, 135.15, 127.58, 127.23, 125.25, 121.74, 83.95, 70.75, 24.82.

HRMS (ESI): *m/z* Calcd for $C_{20}H_{22}BNO_7Na$, $[M+Na]^+$:422.1387, found: 422.1367.

4.4. Compound 8a

To a solution of doxorubicine hydrochloride (10 mg, 0.017 mmol) in 1 mL of DMF was added Et_3N (2.4 µL, 0.017 mmol). The mixture was stirred for 30 min at r.t. before adding HOBt (2.3 mg, 0.017 mmol) and a solution of **7a** (6.8 mg, 0.017 mmol) in 1 mL of DMF and the resulting mixture was stirred a r.t. during 3 h. The reaction was quenched with brine, extracted with DCM (3 × 20 mL), the organic layers were combined, dried with $MgSO_4$ and concentrated under reduced pressure. The crude product was purified over silica gel with DCM-MeOH: 90-10 to give the expected product (10 mg, yield: 78%).

^{1}H NMR (300 MHz, $CDCl_3$) δ 13.96 (s, 1H), 13.20 (s, 1H), 8.02 (d, J = 7.6 Hz, 1H), 7.82–7.73 (m, 3H), 7.42–7.36 (m, 1H), 7.29 (d, J = 9.5 Hz, 2H), 5.51 (d, J = 2.5 Hz, 1H), 5.23 (dd, J = 17.3, 8.8 Hz, 2H), 5.04 (s, 2H), 4.77 (s, 2H), 4.57 (s, 1H), 4.15 (d, J = 6.5 Hz, 1H), 4.08 (s, 3H), 3.88 (s, 1H), 3.68 (s, 1H), 3.25 (d, J = 18.9 Hz, 1H), 2.97 (d, J = 7.5 Hz, 1H), 2.91 (d, J = 10.7 Hz, 1H), 2.33 (d, J = 14.4 Hz, 1H), 2.16 (dd, J = 14.7, 3.7 Hz, 2H), 1.33 (s, 12H), 1.24 (s, 3H). ^{13}C NMR (75 MHz, $CDCl_3$) δ 214.03, 187.14, 186.74, 161.13, 156.29, 155.71, 155.60, 139.46, 135.88, 135.55, 135.07, 133.68, 127.23, 120.90, 119.94, 118.55, 111.65, 111.48, 100.87, 83.93, 69.79, 69.65, 67.41, 66.74, 65.68, 56.77, 47.12, 45.94, 35.72, 34.07, 30.27, 29.81, 24.95, 16.97. HRMS (ESI): *m/z* Calcd for $C_{41}H_{46}BNO_{15}Na$, $[M+Na]^+$: 826.2858, found: 826.2860.

4.5. Compound 6c

To a solution of boronic acid **5** (3.5 mmol, 500 mg) in anhydrous THF (15 mL) was added and pinacol (3.5 mmol, 416 mg). The resulting solution was evaporated under reduced pressure at 40 °C. This procedure was repeated until TLC analysis indicated a complete conversion. The crude product was purified by column chromatography over silica gel with hexane-EtOAc: 90–10 to 50–50 to give the expected product (618 mg, yield: 79%).

^{1}H NMR (300 MHz, $CDCl_3$) δ 7.02 (d, J = 3.3 Hz, 1H), 6.34 (d, J = 3.3 Hz, 1H), 4.66 (s, 2H), 1.34 (s, 12H). ^{13}C NMR (75 MHz, $CDCl_3$) δ 159.07, 124.32, 108.44, 84.17, 75.02, 57.56, 24.62. HRMS (ESI): *m/z* Calcd for $C_{11}H_{17}BO_4Na$, $[M+Na]^+$: 247.1117, found: 247.1114.

4.6. Compound 7b

To a solution of 4-nitrophenyl chloroformate (175 mg, 0.87 mmol) in 5 mL of DCM at 0 °C was added pyridine (68 µL, 0.87 mmol), the solution was stirred during 5 min at 0 °C then a solution of **6b** [39] (73 mg, 0.29 mmol) in 1 mL of DCM was added dropwise to the mixture and the reaction was stirred at r.t. overnight. The reaction was then quenched with a saturated solution of $NaHCO_3$, the aqueous layer was extracted with EtOAc (3 × 20 mL), the organic layers were combined, washed with brine, dried with $MgSO_4$, and concentrated under reduced pressure to give a crude product. The crude product was purified by column chromatography over silica gel with Cyclohexane-EtOAc: 95–5 to 60–40 to give the expected product (25 mg, yield: 20%).

^{1}H NMR (300 MHz, $CDCl_3$) δ 8.34 (dd, J = 1.7; 7.2 Hz, 2H), 8.27 (dd, J = 1.7; 7.2 Hz, 2H), 7.63–7.59 (m, 1H), 7.52–7.50 (m, 1H), 7.40–7.38 (m, 1H), 5.38 (s, 2H), 1.35 (s, 12H). ^{13}C NMR (75 MHz, $CDCl_3$) δ 162.05, 159.20, 152.30, 145.40, 130.10, 125.40, 125.30, 124.10, 121.70, 121.60, 121.20, 64.60, 24.70. HRMS (ESI): *m/z* Calcd for $C_{20}H_{21}BFNO_7Na$, $[M+Na]^+$: 440.1292, found: 440.1276.

4.7. Compound 7c

To a solution of 4-nitrophenyl chloroformate (504 mg, 2.5 mmol) in 15 mL of DCM was added DMAP (54 mg, 0.44 mmol) and the reaction was stirred et 0 °C during 15 min. In another round bottom flask, a solution **6c** (500 mg, 2.2 mmol) and Et_3N (612 µL, 4.4 mmol) in 15 mL of DCM was stirred at 0 °C. The second mixture was added dropwise on the first mixture to give a yellow solution. The solution was stirred during 6 h at r.t. before being quenched with water. The aqueous layer was extracted with DCM (3 × 20 mL), the organic layers were combined, washed with brine, dried with $MgSO_4$, and concentrated under reduced pressure to give a crude product. The crude product was purified by column chromatography over silica gel with DCM-MeOH: 100-0 to 90-10 to give the expected product (250 mg, yield: 30%).

^{1}H NMR (300 MHz, $CDCl_3$) δ 8.24–8.17 (m, 2H), 7.07 (d, J = 3.3 Hz, 1H), 7.05–6.98 (m, 2H), 6.51 (d, J = 3.3 Hz, 1H), 5.14 (s, 2H), 1.36 (s, 12H). ^{13}C NMR (75 MHz, $CDCl_3$) δ 163.12, 153.56, 126.22, 125.90, 124.04, 115.62, 114.69, 113.20, 111.12, 84.48, 62.91, 24.72. HRMS (ESI): *m/z* Calcd for $C_{18}H_{20}BNO_8Na$, $[M+Na]^+$: 412.1179, found: 412.1161.

4.8. Compound 8b

To a solution of doxorubicin hydrochloride (35 mg, 0.06 mmol) in 7 mL of DMF was added Et_3N (8 µL, 0.06 mmol). The mixture was stirred for 30 min at r.t. before adding HOBt (8 mg, 0.06 mmol) and a solution of **7b** (25 mg, 0.06 mmol) in 2 mL of DMF and the resulting mixture was stirred a r.t. during 6 h. The reaction was quenched with brine, the aqueous layer was extracted with extracted with DCM (3 × 20 mL), the organic layers were combined, dried with $MgSO_4$ and concentrated under reduced pressure. The crude product was purified over silica gel with DCM-MeOH: 90-10 to give the expected product

(30 mg, yield: 60%).

^{1}H NMR (300 MHz, $CDCl_3$) δ 13.94 (s, 1H), 13.25 (s, 1H), 8.02 (d, J = 7.4 Hz, 1H), 7.80 (t, J = 8.6 Hz, 1H), 7.41 (d, J = 8.6 Hz, 1H), 7.23 (d, J = 10.4 Hz, 3H), 5.60 (t, J = 7.2 Hz, 1H), 5.35 (s, 1H), 5.21 (s, 1H), 4.77 (s, 2H), 4.54 (d, J = 8.6 Hz, 1H), 4.25 (d, J = 10.3 Hz, 1H), 4.09 (s, 4H), 3.68 (s, 1H), 3.28 (d, J = 21.8 Hz, 2H), 3.10–2.90 (m, 2H), 2.55 (d, J = 13.2 Hz, 1H), 2.24–2.11 (m, 2H), 1.65– 1.50 (m, 6H), 1.35–1.20 (m, 12H). ^{13}C NMR (75 MHz, $CDCl_3$) δ 161.05, 156.14, 15.70, 135.85, 135.50, 133.80, 133.30, 120.86, 119.90, 118.50, 111.60, 99.00, 75.80, 69.30, 65.45, 64.60, 56.70, 47.60, 35.90, 33.80, 29.70, 29.50, 15.80. HRMS (ESI): m/z Calcd for $C_{41}H_{45}BFNO_{15}Na$, $[M+Na]^+$: 844.2764, found: 844.2749.

4.9. Compound 8c

To a solution of doxorubicin hydrochloride (19 mg, 0.033 mmol) in 4 mL of DMF was added Et_3N (4 μL, 0.033 mmol). The mixture was stirred for 30 min at r.t. before adding HOBt (5 mg, 0.033 mg) and a solution of **7c** (13 mg, 0.033 mmol) in 1 mL of DMF. The resulting solution was stirred at r. t. overnight before being quenched with brine, extracted with DCM (3 × 20 mL), the organic layers were combined, dried with $MgSO_4$ and concentrated under reduced pressure. The crude product was purified over silica gel with DCM-MeOH: 90-10 to give the expected product (15 mg, yield: 60%).

^{1}H NMR (300 MHz, $CDCl_3$) δ 13.95 (s, 1H), 13.22 (s, 1H), 8.07 (d, J = 9.1 Hz, 1H), 7.78 (t, J = 8.1 Hz, 1H), 7.38 (d, J = 8.1 Hz, 1H), 6.87 (d, J = 9.0 Hz, 1H), 5.49 (d, J = 3.4 Hz, 1H), 5.27 (s, 1H), 5.10 (d, J = 8.7 Hz, 1H), 4.76 (s, 2H), 4.56 (s, 1H), 4.07 (s, 6H), 3.84 (s, 1H), 3.72–3.59 (m, J = 9.2, 5.9 Hz, 1H), 3.26 (dd, J = 18.9, 1.4 Hz, 1H), 2.97 (s, 3H), 2.89 (s, J = 4.3 Hz, 3H), 2.33 (d, J = 14.6 Hz, 1H), 2.22–2.11 (m, 2H), 1.91–1.70 (m, 2H), 1.37–1.13 (m, 12H). ^{13}C NMR (75 MHz, $CDCl_3$) δ 212.84, 186.08, 185.64, 161.86, 161.73, 160.01, 155.16, 154.93, 154.60, 139.80, 134.79, 134.44, 132.54, 125.04, 119.79, 118.84, 117.43, 114.59, 110.53, 110.36, 99.71, 68.57, 66.30, 64.52, 59.99, 55.65, 52.70, 45.84, 35.62, 34.62, 32.83, 30.55, 29.18, 28.66, 28.20, 23.80, 23.69, 21.66, 15.82, 13.50. HRMS (ESI): m/z Calcd for $C_{39}H_{44}BNO_{16}Na$, $[M+Na]^+$: 816.2650, found: 816.2832.

4.10. Compound 9

To a solution of **7a** (30 mg, 0.075 mmol) in 7 mL of DMF was added Et_3N (11 μL, 0.075 mmol). The mixture was stirred for 30 min at r.t. before adding HOBt (11 mg, 0.075 mg) and a solution of phenylalanine (12.4 mg, 0.075 mmol) in 3 mL of DMF and the resulting mixture was stirred at r.t. overnight. The reaction was quenched with brine, extracted with DCM (3 × 20 mL), the organic layers were combined, dried with $MgSO_4$ and concentrated under reduced pressure. The crude product was purified over silica gel with DCM-MeOH: 90-10 to afford the expected product (220 mg, yield: 89%).

^{1}H NMR (360 MHz, $CDCl_3$) δ 7.79 (d, J = 7.8 Hz, 2H), 7.41–7.19 (m, 5H), 7.14 (d, J = 7.8 Hz, 2H), 5.10 (m, 2H), 4.81–4.60 (m, 1H), 3.36–3.00 (m, 2H), 1.34 (s, 12H).^{13}C NMR (91 MHz, $CDCl_3$) δ 155.80, 139.40, 135.81, 135.42, 132.23, 129.81, 128.58, 127.19, 127.07, 83.88, 66.91, 54.65, 37.81, 29.70, 24.84. HRMS (ESI): m/z Calcd for $C_{23}H_{29}NO_6$, $[M+H]^+$: 426.2086, found: 426.2068.

4.11. Compound 11

To a solution of 4-nitrophenyl chloroformate (745 mg, 3.6 mmol), Et_3N (505 μL, 3.6 mmol) in 4 mL of DCM at 0 °C was added dropwise a solution of 4-(hydroxymethyl)benzoic acid **10** (186 mg, 1.2 mmol) in 4 mL of DCM and 2 mL of DMF. The reaction was stirred at r. t. for 7 h30. The reaction was quenched with $NaHCO_3$, the aqueous layer was extracted with DCM (3 × 20 mL), the organic layers were combined, dried with $MgSO_4$, and concentrated under reduced pressure. The crude product was purified over silica gel with cyclohexane-EtOAc: 100-0 to 60-40 to give the expected product (217 mg, yield: 74%).

^{1}H NMR (300 MHz, $CDCl_3$) δ 8.33–8.26 (m, 4H), 7.46–7.36 (m, 4H), 5.42 (s, 2H). ^{13}C NMR (75 MHz, $CDCl_3$) δ 163.69, 155.52, 152.36, 145.52, 140.56, 130.80, 129.00, 128.30, 125.33, 122.58, 69.76. HRMS (ESI): m/z Calcd for $C_{15}H_{10}NO_7$, $[M-H]^+$: 316.0457, found: 316.0456.

4.12. Compound 12

To a solution of doxorubicin hydrochloride (20 mg, 0.034 mmol) in 5 mL of DMF was added Et_3N (5 μL, 0.034 mmol). The mixture was stirred for 30 min at r.t. before adding HOBt (5 mg, 0.034 mg) and a solution of **11** (11 mg, 0.034 mmol) in 2 mL of DMF and the resulting mixture was stirred a r.t. overnight. The reaction was quenched with brine, extracted with DCM (3 × 20 mL), the organic layers were combined, dried with $MgSO_4$ and concentrated under reduced pressure. The crude product was purified over silica gel with DCM-MeOH: 90-10 to afford the expected product (19 mg, yield: 73%).

^{1}H NMR (300 MHz, $(CD_3)_2SO$) δ 13.97 (d, J = 7.4 Hz, 1H), 13.20 (d, J = 5.0 Hz, 1H), 7.93 (d, J = 7.8 Hz, 1H), 7.83 (m, 2H), 7.75 (d, J = 7.8 Hz, 1H), 7.58 (d, J = 7.4 Hz, 1H), 7.32 (d, J = 7.4 Hz, 1H), 6.97 (s, 1H), 5.44 (d, J = 13.3 Hz, 1H), 5.22 (d, J = 13.3 Hz, 1H), 4.97 (s, 1H), 4.94–4.80 (m, 2H), 4.73 (d, J = 7.4 Hz, 1H), 4.65–4.50 (m, 2H), 4.30–4.10 (m, 2H), 3.94 (s, 3H), 4.97 (s, 1H) ^{13}C NMR (75 MHz, $(CD_3)_2SO$) δ 213.90, 188.36, 186.45, 186.36, 160.74, 156.13, 155.20, 154.52, 154.06, 140.23, 136.20, 135.51, 134.58, 134.05, 133.92, 127.44, 126.99, 119.90, 119.69, 118.97, 110.72, 110.59, 101.67, 100.53, 100.36, 74.96, 70.01, 69.89, 67.94, 66.67, 63.75, 56.56, 17.06. HRMS (ESI): m/z Calcd for $C_{36}H_{35}NO_{15}Na$, $[M+Na]^+$: 744.1904, found: 744.1901.

4.13. H_2O_2 activation of the profluorescent probe

Carbon-boron bond oxidation by ROS (i.e·H_2O_2) was studied using the arylboronate profluorescent probe **3** in presence of increasing H_2O_2 concentration at r.t. The study was fulfilled in 96 well black plates (Corning) by mixing **3** in DMSO/10 mM Hepes buffer (pH 7.5) (1/99) at a final concentration of 50 μM in presence of increasing amount of H_2O_2: 1, 5, 10 and 50 equivalents (i.e. 50, 250, 500 and 2 500 μM, final concentration). The coumarin release kinetic was studied over 12 h by reading its fluorescence intensity at $\lambda_{excitation}/\lambda_{emission}$: 390/500 nm every 5 min for the first hour and every 30 min during the eleven remaining hours (Infinite M200 Pro, Tecan trading AG, Switzerland). The final fluorescent intensity was calculated by subtracting the minor fluorescence of **3** in absence of H_2O_2 to the fluorescence obtained in presence of H_2O_2. The curves relating the release kinetic of coumarin were obtained using GraphPad Prism software (GraphPad Software Inc, San Diego, CA, USA).

4.14. Cell line and culture

Several cancer cell lines have been used for the in vitro evaluation of the designed prodrugs in comparison to the parent drug: doxorubicin (DOX). Six cell lines were selected for the cytotoxicity assay as follows: U87 (glioblastoma), A549 (lung carcinoma), MCF-7 (breast cancer), MCF-7 MDR (multi drug resistant breast cancer), MiaPaCa-2 (pancreatic cancer) and Hep G2 (liver cancer). All cells were grown in DMEM (Dulbecco's Modified Eagle Medium) supplemented with 10% of fetal calf serum (FCS) and 100 U/mL penicillin and 100 μg/mL streptomycin (Invitrogen) in a 5% CO_2 and 95% hygrometry environment at 37 °C.

4.15. In vitro screening

All seven cell line were investigated for their ability to produce ROS using profluorescent probe **3**. Six well plates were used for this study, each well was seeded with 5.10^5 cell per well and treated with 10 μM of

3 (sixplicate). After a 6 h incubation period at 37 °C in presence 5% CO_2 and 95% hygrometry, each well was sonicated three times during 5 s (Sonicator FB505, Fisher Scientific, USA) and 100 µL of the supernatant was transferred in a 96 well black plate. The fluorescence of each well was then read at the coumarin fluorescence wavelength $\lambda_{excitation}$/$\lambda_{emission}$: 390/500 nm to measure its release reflecting the ability of each cell line to produce ROS. This study was carried out in triplicate and the results of each cell line was compared to the cell line producing the least ROS (U87) results using a non-parametric Kruskall-Wallis test ($p < 0.001$) with GraphPad Prism software (GraphPad Software Inc, San Diego, CA, USA). A p value of < 0.0001 was accepted as statistically significant.

4.16. In vitro cell-proliferation assay

The cytotoxic activity of all the designed prodrugs and controls (**8a**, **8b**, **8c**, **9** and **12**) was investigated using the MTS [(3-(4,5-dimethylthiazol-2-yl)-5-(3-carboxymethoxyphenyl)-2-(4-sulfophenyl)-2*H*-tetrazolium)] method (Promega). The cells (2 500, 7 000, 7 000, 5 000, 5 000, 7 000 and 10 00 cell per well for A549, MCF-7, MCF-7 MDR, MiaPaCa-2, U87 and Hep G2, respectively) (100 µL) were seeded in 96-well plates and incubated overnight at 37 °C in presence 5% CO_2 and 95% hygrometry. Then, the cells were treated with 100 µL of each compound at different concentrations (i.e. 0.0025, 0.005, 0.025, 0.05, 0.25, 0.5, 2.5, 5, 25, 50 µM, final concentration) for all the tested cell lines. After 72 h, 20 µL (1/10) of MTS reagent were added in each well. Depending on the cell line, 2 to 5 h incubations at 37 °C in presence 5% CO_2 and 95% hygrometry were needed to obtain the optimum optical density which was measured at 490 nm wavelength using a microplate reader (Infinite M200 Pro, Tecan trading AG, Switzerland). Untreated cells were used as control. Each concentration was tested in six replicates and the experiment was fulfilled in triplicates. The concentration inhibiting 50% of the cell proliferation (IC_{50}) was determined using GraphPad Prism software (GraphPad Software Inc, San Diego, CA, USA).

4.17. Chick chorioallantoic membrane assay (CAM assay)

Fertilized white leghorn chicken eggs (E.A.R.L. Morizeau, Dangers, France) were maintained at 24 °C before hatching. Eggs were subsequently hatched in a humidified incubator (Sailnovo 56A incubator) at 37 °C and 70% hygrometry. The initial day of incubation is considered day 0. At day 10, all eggs were mired and the air sac was visualized and delimited. The shell was cautiously cut near the air sac position to visualize the egg membrane. The egg membrane was homogeneously moisturized with NaCl 0.9% solution and left 5 min. The solution was then aspirated and the egg membrane was carefully removed revealing the chorioallantoic membrane (CAM). Prior to implantation on the CAM, MiaPaCa-2 cell suspensions were prepared by detaching them with trypsin/EDTA followed by their counting. Cells were centrifuged at 1200 rpm for 5 min, washed twice using DMEM without FCS and suspended in a mix of Matrigel (ECM Matrigel, Sigma) and DMEM (75/25) at a final concentration of 5.10^7 cell per mL. 1.10^6 MiaPaCa-2 cells (20 µL) were deposited onto the CAM, without allowing the pipette tip to touch the CAM. The window was then sealed using adhesive plaster to prevent dehydration. The eggs were incubated (without shaking) awaiting the tumor to grow. After approximately three days, tumor were visible and the treatment could take place. The tumors were treated by intratumoral injections of DOX and **8a** at different doses either as a single injection (184 nmol) or twice a day for two consecutive days (20 nmol/injection). In ovo tumors were photographed three days post-treatment using an Olympus digital camera 15.9 mega pixel using the macro feature (OM-D E-M5). Image treatment and tumor measurements were carried out using FIJI software [43]. The tumor were then taken out carefully and suspended in 1 mL of PBS before being sonicated to dissociate the tumor. After centrifugation at 1200 rpm for 5 min, the supernatant was filtered before being analyzed by HPLC.

4.18. HPLC detection of doxorubicin

HPLC analysis was used to estimate the doxorubicin release within the tumor collected for the HET-CAM assay using a gradient method composed of acetonitrile as the phase A and water containing 0.1% of formic acid as phase B. The HPLC separation was carried on a 1260 infinity HPLC system (Agilent Technologies, United Kingdom). The chromatographic separation was carried out on a Kinetex® 5 µm C18 (250 × 4.6 mm) LC column at a flow rate of 1.0 mL/min. A gradient elution was used with initially 10% acetonitrile which was increased linearly to 30% over 4 min, then increased to 80% over 2 min and remained at this condition for 6 min before being finally decreased to 10% in 3 min and was held until the end of the 20 min run. All analyses were performed at 30 °C. The mobile phase were filtered and degassed in an ultrasonic bath before use. The retention times of DOX and **8a** in these conditions of analysis were 9.03 and 9.85 min, respectively.

Acknowledgements

This work was funded by the “Comité Essonne de la Ligue Nationale Contre le Cancer” and the “Fondation ARC pour la recherche sur le cancer”. C. Skarbek is financed by a postdoctoral training grant from the “Fondation ARC pour la recherche sur le cancer”. S. Serra was a “Ligue Nationale Contre le Cancer” postdoctoral fellow. H. Maslah is supported by the “Ministère de l’Education Nationale de la Recherche et de la Technologie”. Pierre Milcendeau is acknowledged for technical assistance on organic synthesis.

References

[1] Cancer Research UK, https://www.cancerresearchuk.org/health-professional/cancer-statistics/worldwide-cancer#heading-One, (accessed in May 2019).
[2] J. Rautio, N.A. Meanwell, L. Di, M.J. Hageman, Nat. Rev. Drug Discov. 17 (2018) 559–587.
[3] V. Taresco, C. Alexander, N. Singh, A.K. Pearce, Adv. Therap. 1 (2018) 1800030.
[4] D. Trachootham, J. Alexandre, P. Huang, Nat. Rev. Drug Discov. 8 (2009) 579–591.
[5] G.Y. Liou, P. Storz, Free Radical Res. 44 (2010) 479–496.
[6] N. Nishida, H. Yano, T. Nishida, T. Kamura, M. Kojiro, Vasc. Health Risk Manage. 2 (2006) 213–219.
[7] X. Peng, V. Gandhi, Ther. Deliv. 3 (2012) 823–833.
[8] J.P. Cadahía, V. Previtali, N.S. Troelsen, M.H. Clausen, Med. Chem. Commun. (2019), https://doi.org/10.1039/C9MD00169G.
[9] S.J. Baker, C.Z. Ding, T. Akama, Y.K. Zhang, V. Hernandez, Y. Xia, Fut. Med. Chem. 1 (2009) 1275–1288.
[10] A. Alouane, R. Labruère, T. Le Saux, F. Schmidt, L. Jullien, Angew. Chem. Int. Ed. 54 (2015) 7492–7509.
[11] G.C. van de Bittner, E.A. Dubikovskaya, C.R. Bertozzi, C.J. Chang, Proc. Natl. Acad. Sci. USA 107 (2010) 21316–21321.
[12] D. Andina, J.-C. Leroux, P. Luciani, Chem. Eur. J. 23 (2017) 13549–13573.
[13] H. Hagen, P. Marzenell, E. Jentzsch, F. Wenz, M.R. Veldwijk, A. Mokhir, J. Med. Chem. 55 (2012) 924–934.
[14] S. Daum, M.S.V. Reshetnikov, M. Sisa, T. Dumych, M.D. Lootsik, R. Bilyy, E. Bila, C. Janko, C. Alexiou, M. Herrmann, L. Sellner, A. Mokhir, Angew. Chem. Int. Ed. Engl. 56 (2017) 15545–15549.
[15] J. Noh, B. Kwon, E. Han, M. Park, W. Yang, W. Cho, W. Yoo, G. Khang, D. Lee, Nat. Commun. 6 (2015) 6907.
[16] S. Cao, Y. Wang, X. Peng, Chem. Eur. J. 18 (2012) 3850–3854.
[17] Y. Wang, H. Fan, K. Balakrishnan, Z. Lin, S. Cao, W. Chen, Y. Fan, Q.A. Guthrie, H. Sun, K.A. Teske, V. Gandhi, L.A. Arnold, X. Peng, Eur. J. Med. Chem. 133 (2017) 197–207.
[18] J.L. Major Jourden, S.M. Cohen, Angew. Chem. Int. Ed. Engl. 49 (2010) 6795–6797.
[19] Y. Kuang, K. Balakrishnan, V. Gandhi, X. Peng, J. Am. Chem. Soc. 133 (2011) 19278–19281.
[20] W. Chen, H. Fan, K. Balakrishnan, Y. Wang, H. Sun, Y. Fan, V. Gandhi, L.A. Arnold, X. Peng, J. Med. Chem. 61 (2018) 9132–9145.
[21] E.J. Kim, S. Bhuniya, H. Lee, H.M. Kim, C. Cheong, S. Maiti, K.S. Hong, J.S. Kim, J. Am. Chem. Soc. 136 (2014) 13888–13894.
[22] L. Wang, S. Xie, L. Ma, Y. Chen, W. Lu, Eur. J. Med. Chem. 116 (2016) 84–89.
[23] Q. Jiang, Q. Zhong, Q. Zhang, S. Zheng, G. Wang, ACS Med. Chem. Lett. 3 (2012) 392–396.
[24] C. Zhang, Q. Zhong, Q. Zhang, S. Zheng, L. Miele, G. Wang, Breast Cancer Res. Treat. 152 (2015) 283–291.

[25] J. Peiró Cadahía, J. Bondebjerg, C.A. Hansen, V. Previtali, A.E. Hansen, T.L. Andresen, M.H. Clausen, J. Med. Chem. 61 (2018) 3503–3515.
[26] V. Reshetnikov, S. Daum, A. Mokhir, Chem. Eur. J. 23 (2017) 5678–5681.
[27] S. Zheng, S. Guo, Q. Zhong, C. Zhang, J. Liu, L. Yang, Q. Zhang, G. Wang, ACS Med. Chem. Lett. 9 (2018) 149–154.
[28] Y. Liao, L. Xu, S. Ou, H. Edwards, D. Luedtke, Y. Ge, Z. Qin, ACS Med. Chem. Lett. 9 (2018) 635–640.
[29] Y. Ai, O.N. Obianom, M. Kuser, Y. Li, Y. Shu, F. Xue, ACS Med. Chem. Lett. 10 (2018) 127–131.
[30] M. Ye, Y. Han, J. Tang, Y. Piao, X. Liu, Z. Zhou, J. Gao, J. Rao, Y. Shen, Adv. Mater. 29 (2017) 1702342.
[31] Y. Octavia, C.G. Tocchetti, K.L. Gabrielson, S. Janssens, H.J. Crijns, A.L. Moens, J. Mol. Cell Cardiol. 52 (2012) 1213–1225.
[32] S. Cao, R. Christiansen, X. Peng, Chem. Eur. J. 19 (2013) 9050–9058.
[33] M.P. Hay, R.F. Anderson, D.M. Ferry, W.R. Wilson, W.A. Denny, J. Med. Chem. 46 (2003) 5533–5545.
[34] C.S. Kue, K.Y. Tan, M.L. Lam, H.B. Lee, Exp. Anim. 64 (2015) 129–138.
[35] N.A. Lokman, A.S. Elder, C. Ricciardelli, M.K. Oehler, Int. J. Mol. Sci. 13 (2012) 9959–9970.
[36] M. Taizi, V.R. Deutsch, A. Leitner, A. Ohana, S. Goldstein, Exp. Hematol. 34 (2006) 1698–1708.
[37] M. Hagedorn, S. Javerzat, D. Gilges, A. Meyre, B. De Laforge, A. Eichmann, A. Bikfalvi, Proc. Natl. Acad. Sci. USA 102 (2005) 1643–1648.
[38] M. Balke, A. Neumann, C. Kersting, K. Agelopoulos, C. Gebert, G. Gosheger, H. Buerger, M. Hagedorn, BMC Res. Notes 3 (2010) 58.
[39] G.B. Atallah, W. Chen, D. Khrakovsky, L. Wang, Z.J. Jia, F. Jr Deanda. U.S. Pat. Appl. Publ. (2018), US 20180194762 A1 20180712.
[40] J. Zielonka, A. Sikora, M. Hardy, J. Joseph, B.P. Dranka, B. Kalyanaraman, Chem. Res. Toxicol. 25 (2012) 1793–1799.
[41] A. Alouane, R. Labruère, T. Le Saux, I. Aujard, S. Dubruille, F. Schmidt, L. Jullien, Chem. Eur. J. 19 (2013) 11717–11724.
[42] C.M. Doskey, V. Buranasudja, B.A. Wagner, J.G. Wilkes, J. Du, J.J. Cullen, G.R. Buettner, Redox Biol. 10 (2016) 274–284.
[43] J. Schindelin, I. Arganda-Carreras, E. Frise, V. Kaynig, M. Longair, Pietzsch, S. Preibisch, C. Rueden, S. Saalfeeld, B. Schmid, J.-Y. Tinevez, D.J. White, V. Hartenstein, K. Eliceiri, P. Tomancak, Nat. Methods 9 (2012) 676–682.